Analytical Solutions for Transient Temperature of Semi-Infinite Body Subjected to 3-D Moving Heat Sources

Article in Welding Journal · August 1999						
CITATIONS		READS				
137		413				
5 author	s, including:					
106	Ninh T Nguyen					
	HRL Technology Group					
	75 PUBLICATIONS 710 CITATIONS					
	SEE PROFILE					
Some of the authors of this publication are also working on these related projects:						
Project	Ninh Nguyen View project					
Project	NN PhD Project View project					

WELDING RESEARCH





SUPPLEMENT TO THE WELDING JOURNAL, AUGUST 1999
Sponsored by the American Welding Society and the Welding Research Council

Analytical Solutions for Transient Temperature of Semi-Infinite Body Subjected to 3-D Moving Heat Sources

Analytical solutions for 3-D moving heat sources were derived and experimentally validated by transient temperature measured at various points in bead-on-plate specimens and by means of weld pool geometry

BY N. T. NGUYEN, A. OHTA, K. MATSUOKA, N. SUZUKI AND Y. MAEDA

ABSTRACT. The analytical solution for a double-ellipsoidal power density moving heat source in a semi-infinite body with conduction-only consideration has been derived. The solution has been obtained by integrating the instant point heat source throughout the volume of the ellipsoidal one. Very good agreement between the predicted transient temperatures and the measured ones at various points in bead-on-plate specimens has been obtained. The predicted geometry of the weld pool is also in good agreement with the measured one. This may pave the way for the future applications of this solution in the problems such as microstructure modeling, thermal stress analysis, residual stress/distortions and welding process simulation.

Introduction

The temperature history of the welded components has a significant influence on the residual stresses, distortion and hence the fatigue behavior of the welded structures. Classical solutions for the transient temperature field such as Rosenthal's solutions (Ref. 1) dealt with the semi-infinite body subjected to an instant point heat source, line heat source

N. SUZUKI, Y. MAEDA, N. T. NGUYEN and A. OHTA are with National Research Institute for Metals (NRIM), Ibaraki, Japan. K. MAT-SUOKA is with Ship Research Institute, Shinkawa, Tokyo, Japan. or surface heat source. These solutions can be used to predict the temperature field at a distance far from the heat source but fail to predict the temperature in the vicinity of the heat source.

Eagar and Tsai (Ref. 2) modified Rosenthal's theory to include a two-dimensional (2-D) surface Gaussian distributed heat source with a constant distribution parameter (which can be considered as an effective arc radius) and found an analytical solution for the temperature of a semi-infinite body subjected to this moving heat source. Their solution is a significant step for the improvement of temperature prediction in the near heat source regions.

Jeong and Cho (Ref. 3) introduced an analytical solution for the transient temperature field of a fillet-welded joint based on the similar 2-D Gaussian heat

KEY WORDS

Transient Heat Source Three-Dimensional Temperature Field Moving Heat Source Gaussian Two-Dimensional Thermal Stress source but with different distribution parameters (in two directions x and y). Using the conformal mapping technique, they have successfully transformed the solution of the temperature field in the plate of a finite thickness to the fillet welded joint. Even though the available solutions using the Gaussian heat sources could predict the temperature at regions closed to the heat source, they are still limited by the shortcoming of the 2-D heat source itself with no effect of penetration. This shortcoming can only be overcome if more general heat sources are implemented.

Goldak, et al. (Ref. 4), first introduced the three-dimensional (3-D) double ellipsoidal moving heat source. Finite element modeling (FEM) was used to calculate the temperature field of a bead-on-plate and showed that this 3-D heat source could overcome the shortcoming of the previous 2-D Gaussian model to predict the temperature of the welded joints with much deeper penetration. However, up to now, an analytical solution for this kind of 3-D heat source was not yet available (Ref. 5), and hence, researchers must rely on FEM for transient temperature calculation or other simulation purposes, which requires the thermal history of the components. Therefore, if any analytical solution for a temperature field from a 3-D heat source is available, a lot of CPU time could be saved and the thermal-stress

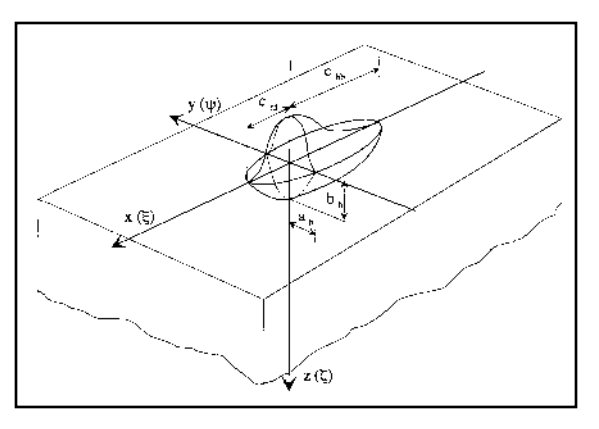


Fig. 1 — Double ellipsoidal density distributed heat source.

analysis or related simulations could be carried out much more rapidly and conveniently.

In this study, analytical solutions for the transient temperature field of the semi-infinite body subjected to 3-D power density moving heat sources (such as semi-ellipsoidal and double ellipsoidal heat sources) are derived and reported. The calculated transient temperatures at various points of interest in a steel plate, 240 x 240 x 20 mm, subjected to two perpendicular linear welded segments on its surface, are compared with the measured data by the authors. The geometry of the weld pool was also measured and compared with the predicted one. Reasonably good agreements between the calculated and measured data show a potential application of this newly developed solution for various simulation purposes such as thermal stress analysis or residual stress calculations.

Ellipsoidal Heat Sources in Semi-Infinite Body

Goldak's Semi-Ellipsoidal Heat Source

Goldak, et al. (Ref. 4), initially proposed a semi-ellipsoidal heat source in which heat flux is distributed in a Gaussian manner throughout the heat source's volume. The heat flux Q(x,y,z) at a point (x,y,z) within the semi-ellipsoid is given by the following equation:

$$Q(x, y, z) = \frac{6\sqrt{3\eta \cdot V \cdot I}}{a_h b_h c_h \pi \sqrt{\pi}}$$
$$\exp\left(-\frac{3x^2}{c_h^2} - \frac{3y^2}{a_h^2} - \frac{3z^2}{b_h^2}\right)$$

where a_h,b_h,c_h = ellipsoidal heat source parameters as described in Fig. 1, where $c_{hf} = c_{hb} = c_h$; x,y,z = moving coordinates of the heat source; Q(x,y,z) = heat flux Q(x,y,z) at a point (x,y,z); V, I and η =

welding voltage and current and arc efficiency.

However, their experience with this heat source showed the predicted temperature gradients in front of the arc were less steep than experimentally observed ones and gradients behind the arc were steeper than those measured. То overcome this, they combined two semiellipsoids and proposed a new heat source called "double ellipsoidal heat source," as shown in Fig. 1.

Goldak's Double Ellipsoidal Heat Source

Since two different semi-ellipsoids are combined to give the new heat source, the heat flux within each semi-ellipsoid are described by different equations.

For a point (x,y,z) within the first semiellipsoid located in front of the welding arc, the heat flux equation is described as

$$Q(x, y, z) = \frac{6\sqrt{3}r_f Q}{a_h b_h c_{hf} \pi \sqrt{\pi}}$$

$$\exp\left(-\frac{3x^2}{c_{hf}^2} - \frac{3y^2}{a_h^2} - \frac{3z^2}{b_h^2}\right)$$
(2)

and for points (*x*,*y*,*z*) within the second semi-ellipsoid, covering the rear section of the arc, as

$$Q(x, y, z) = \frac{6\sqrt{3}r_b Q}{a_h b_h c_{hb} \pi \sqrt{\pi}}$$

$$\exp\left(-\frac{3x^2}{c_{hb}^2} - \frac{3y^2}{a_h^2} - \frac{3z^2}{b_h^2}\right)$$
(3)

where a_h , b_h , c_{hf} , c_{hb} = ellipsoidal heat source parameters as described in Fig. 2; Q = arc heat input ($Q = \eta IV$); r_f , r_b = proportion coefficient representing heat apportionment in front and back of the heat source, respectively, where $r_f + r_b = 2$ (Ref. 4).

It must be noted here that due to the condition of continuity of the volumetric heat source, the values of Q(x,y,z) given by Equations 2 and 3 must be equal at the x = 0 plane. From that condition, another constraint is obtained for r_f and r_b as $r_f/c_{hf} = r_b/c_{hb}$. Subsequently, the values for these two coefficients are determined as $r_f = 2c_{hf}/(c_{hf} + c_{hb})$; $r_b = 2c_{hb}/(c_{hf} + c_{hb})$.

It is worth noting this double ellipsoidal distribution heat source is described by five unknown parameters: the arc efficiency η , and ellipsoidal axis a_h , b_h , c_{hf} and c_{hb} . Goldak, et al. (Ref. 4), implied an equivalence between the source dimensions and those of the weld pool and suggested that appropriate

values for $a_{h,}$ $b_{h,}$ c_{hf} and c_{hb} could be obtained by measurement of the weld pool geometry.

Analytical Solutions

<u>Transient Temperature Field of</u> <u>Semi-Ellipsoidal Heat Source in</u> <u>Semi-Infinite Body</u>

The solution for the temperature field of a semi-ellipsoidal heat source in a semi-infinite body is based on the solution for an instant point source that satisfies the following differential equation of heat conduction in fixed coordinates (Ref. 6)

$$dT_{t'} = \frac{\delta Q dt'}{\rho c \left[4\pi a (t - t') \right]^{3/2}} \cdot \exp \left[-\frac{(x - x')^2 + (y - y')^2 + (z - z')^2}{4a (t - t')} \right]$$
(4)

where a = thermal diffusivity (a = k/cp); c = specific heat; k = thermal conductivity; p = mass density; t, t' = time; dTt' = transient temperature due to the point heat source δQ at time t'; and (x',y',z') = location of the instant point heat source δQ at time t'.

Let us consider the solution of an instant semi-ellipsoidal heat source as a result of superposition of a series of instant point heat sources over the volume of the distributed Gaussian heat source. Substitute Equation 1 for the heat flux at a point source into Equation 4 and integration over the volume of the heat source semi-ellipsoid gives

$$dT_{t'} = \frac{1}{2} \int_{-\infty}^{\infty} dx' \int_{-\infty}^{\infty} dy' \int_{-\infty}^{\infty} dz' \frac{dt'}{\rho c \left[4\pi a (t - t') \right]^{3/2}} \cdot \frac{6\sqrt{3}Q}{a_h b_h c_h \pi \sqrt{\pi}} \cdot \exp \left(-\frac{3x'^2}{c_h^2} - \frac{3y'^2}{a_h^2} - \frac{3z'^2}{b_h^2} \right) \cdot \exp \left(-\frac{(x - x')^2 + (y - y')^2 + (z - z')^2}{4a(t - t')} \right)$$
(5)

Subsequently, by evaluating and simplifying, Equation 5 can be rewritten as

$$dT_{t'} = \frac{3\sqrt{3}Qdt'}{\rho c\pi \sqrt{\pi}} \cdot \frac{1}{\sqrt{12a(t-t') + a_h^2}} \cdot \frac{1}{\sqrt{12a(t-t') + c_h^2}} \cdot \frac{1}{\sqrt{12a(t-t') + c_h^2}} \cdot \frac{1}{\sqrt{12a(t-t') + c_h^2}} \cdot \frac{1}{\sqrt{12a(t-t') + c_h^2}} \cdot \frac{3x^2}{12a(t-t') + a_h^2} - \frac{3z^2}{12a(t-t') + b_h^2}$$

Equation 6 provides the temperature rise

due to a very short time increment dt' from time t' due to amount of heat Qdt' released on the semi-infinite body. When considering a moving heat source with a constant speed v from time t' = 0 to time t' = t, the increase of the temperature during this time is the sum of all of the contribution of the moving heat source during the traveling time. Therefore,

$$\begin{split} T - T_{O} &= \frac{3\sqrt{3}Q}{\rho c \pi \sqrt{\pi}} \cdot \\ \int_{0}^{t} \frac{dt'}{\sqrt{12a(t-t') + a_{h}^{2}} \sqrt{12a(t-t') + b_{h}^{2}} \sqrt{12a(t-t') + c_{h}^{2}}} \cdot \\ &= \exp \left[-\frac{3(x-vt')^{2}}{12a(t-t') + c_{h}^{2}} - \frac{3y^{2}}{12a(t-t') + a_{h}^{2}} - \frac{3z^{2}}{12a(t-t') + b_{h}^{2}} \right] \end{split}$$

where T is temperature at time t and T_o is initial temperature of a point (x,y,z).

Now let us consider several specific cases of the semi-ellipsoidal heat source as follows:

Semi-sphere heat source. If $a_h = b_h = c_h = r_h$, then the semi-ellipsoidal heat source becomes the semi-sphere heat source with radius r_h and Equation 7 becomes

$$T - T_0 = \frac{3\sqrt{3}Q}{\rho c\pi \sqrt{\pi}} \cdot \int_0^t \frac{dt'}{\left[12a(t - t') + r_h^2\right]^{3/2}} \cdot \exp\left(-\frac{3(x - vt')^2 + 3y^2 + 3z^2}{12a(t - t') + r_h^2}\right)$$
(8)

Equation 8 can be simplified further by substituting $r_h = \sqrt{3} \sigma$ (where σ is distribution parameter) as

$$T - T_0 = \frac{Q}{\rho c} \cdot \int_0^t \frac{dt'}{\left[4a(t - t')\right]^{3/2}} \cdot \exp\left(-\frac{(x - vt')^2 + y^2 + z^2}{4a(t - t')}\right)$$
(9)

An Instant Point Source. If $\sigma = 0$, Equation 9 reduces to the temperature distribution for the instant point source as

$$T - T_0 = \frac{Q}{\rho c} \cdot \int_0^t \frac{dt'}{\left[4\pi a(t - t')\right]^{3/2}} \cdot \exp\left(-\frac{(x - vt')^2 + y^2 + z^2}{4a(t - t')}\right)$$
(10)

This solution is consistent with the one published by Carslaw and Jaeger (Ref. 6) as reported previously (Equation 4).

Gaussian Surface-Distributed Heat Source. If $b_h = 0$ ~then the semi-ellipsoidal heat source becomes a Gaussian surface-distributed heat source or Ellipti-

cal disk heat source. In this case Equation 7 can be rewritten as

$$T - T_{o} = \frac{3Q}{\pi\rho c}.$$

$$\int_{0}^{t} \frac{dt'}{\sqrt{4\pi a(t-t')} \sqrt{12a(t-t') + a_{h}^{2}} \sqrt{12a(t-t') + c_{h}^{2}}}.$$

$$\exp \left(-\frac{3(x-vt')^{2}}{12a(t-t') + c_{h}^{2}} - \frac{3y^{2}}{12a(t-t') + a_{h}^{2}} - \frac{z^{2}}{4a(t-t')}\right)$$
(11)

When $a_h=c_h=\sqrt{6} \sigma$, then the elliptical disk heat source becomes a circular disk and Equation 11 becomes

$$T - T_o = \frac{Q}{\pi \rho c}.$$

$$\int_0^t \frac{dt'}{\sqrt{4\pi a(t - t')} \left[4a(t - t') + 2\sigma^2\right]}.$$

$$\exp\left(-\frac{(x - vt')^2 + y^2}{4a(t - t') + 2\sigma^2} - \frac{z^2}{4a(t - t')}\right)$$
(12)

Equation 12 gives the same form as the solution published by Eagar and Tsai (Ref. 2)

Transient Temperature Field of Double Ellipsoidal Heat Source in Semi-Infinite Body

Using a similar approach, an analytical solution for transient temperature of a semi-infinite body subjected to a double ellipsoidal heat source can be obtained as follows:

Let us consider again that the solution for the double ellipsoidal heat source is the superposition of a series of instant point heat sources over the volume of the distributed Gaussian heat source. Substitute Equation 1 for the point source in Equation 4 and take integration over the heat source volume for both front and back portion of the volume heat source. This volume is corresponding to two quadrants of the front and back semi-ellipsoids, respectively, as

$$dT_{t'} = \frac{1}{4} \cdot \frac{6\sqrt{3Qdt'}}{\rho ca_{h}b_{h}\pi\sqrt{\pi} \left[4\pi a(t-t')\right]^{3/2}}$$

$$\int_{-\infty}^{\infty} \int_{-\infty}^{\infty} \exp\left(-\frac{(x-x')^{2} + (y-y')^{2} + (z-z')^{2}}{4a(t-t')}\right)$$

$$\left(\frac{r_{f}}{c_{h}f} \cdot \exp\left(-\frac{3x'^{2}}{c_{h}^{2}f} - \frac{3y'^{2}}{a_{h}^{2}} - \frac{3z'^{2}}{b_{h}^{2}}\right) + \frac{1}{2}\left(\frac{r_{h}}{c_{h}} \cdot \exp\left(-\frac{3x'^{2}}{c_{h}^{2}b} - \frac{3y'^{2}}{a_{h}^{2}} - \frac{3z'^{2}}{b_{h}^{2}}\right)\right) \cdot dx'dy'dz'\right)$$

$$\left(\frac{r_{h}}{c_{h}b} \cdot \exp\left(-\frac{3x'^{2}}{c_{h}^{2}b} - \frac{3y'^{2}}{a_{h}^{2}} - \frac{3z'^{2}}{b_{h}^{2}}\right)\right)$$
(13)

Equation 13 can be simplified further as

$$dT_{t'} = \frac{3\sqrt{3}Qdt'}{2\pi\rho c} \sqrt{\pi \left(12a(t-t') + a_h^2\right) \left(12a(t-t') + b_h^2\right)}$$

$$\left(\frac{A}{\sqrt{12a(t-t')} + c_{hf}^2} + \frac{B}{\sqrt{12a(t-t')} + c_{hf}^2}\right) \qquad (14a)$$

$$where A = r_f \cdot \exp\left(-\frac{3x^2}{12a(t-t') + a_h^2} - \frac{3y^2}{12a(t-t') + b_h^2}\right)$$

$$B = r_b \cdot \exp\left(-\frac{3x^2}{12a(t-t') + c_{hh}^2}\right)$$

$$B = r_b \cdot \exp\left(-\frac{3x^2}{12a(t-t') + a_h^2} - \frac{3y^2}{12a(t-t') + a_h^2}\right) \qquad (14c)$$

$$-\frac{3z^2}{12a(t-t') + a_h^2}$$

Similarly, when considering a moving heat source with a constant speed v from time t' = 0 to time t' = t, the increase of temperature during this time is equivalent to the sum of all the contributions of the moving heat source during the traveling time as

$$T - T_{O} = \frac{3\sqrt{3}Q}{2\rho c\pi \sqrt{\pi}} \int_{0}^{t} \frac{dt'}{\sqrt{\left(12a(t-t') + a_{h}^{2}\right)\left(12a(t-t') + b_{h}^{2}\right)}}$$

$$\left(\frac{A'}{\sqrt{12a(t-t')} + c_{hf}^{2}} + \frac{B'}{\sqrt{12a(t-t')} + c_{hf}^{2}}\right) \qquad (15a)$$

$$\left(-\frac{3(x-vt')^{2}}{12a(t-t') + c_{hf}^{2}}\right)$$

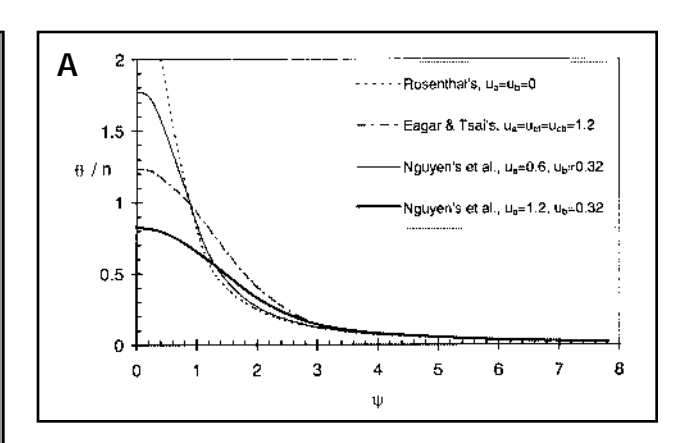
$$where A' = r_{f} \cdot \exp\left[-\frac{3y^{2}}{12a(t-t') + a_{h}^{2}} - \frac{3z^{2}}{12a(t-t') + c_{hh}^{2}}\right]$$

$$\left(-\frac{3(x-vt')^{2}}{12a(t-t') + b_{h}^{2}}\right)$$

$$B' = r_{b} \cdot \exp\left[-\frac{3(x-vt')^{2}}{12a(t-t') + a_{h}^{2}} - \frac{3y^{2}}{12a(t-t') + a_{h}^{2}} - \frac{3z^{2}}{12a(t-t') + b_{h}^{2}}\right]$$

$$(15c)$$

Equations 15a to 15c give the solution for the transient temperature of a semi-infinite body subjected to a double ellipsoidal heat source. It is also worth noting here that Equations 14 and 15 can be easily reduced to the form of Equations 6 and 7, respectively, by substituting $c_{hf} = c_{hb}$ into Equations 14 and 15. This can be expected because in this case the double ellipsoidal heat source becomes the semi-ellipsoidal one.



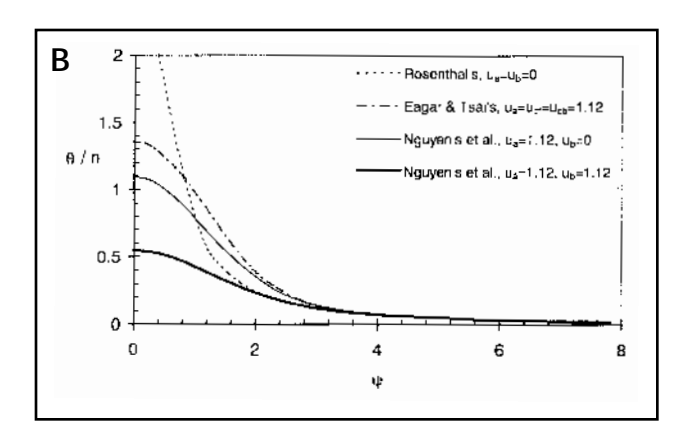
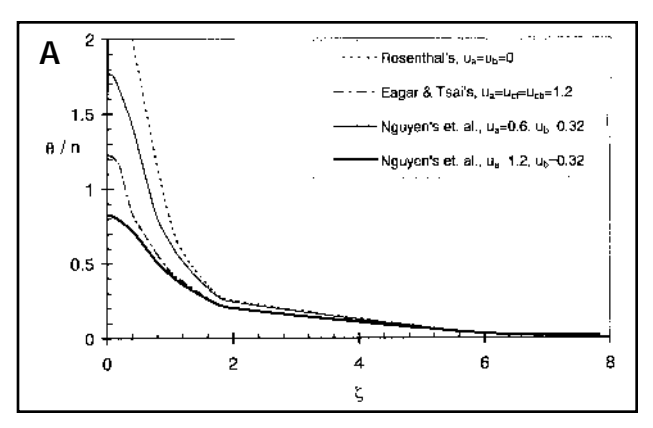


Fig. 2 — Maximum dimensionless temperature distribution along transversal direction ψ . A — The effect of distribution parameter $u_{a'}$ B — the effect of distribution parameter $u_{b'}$



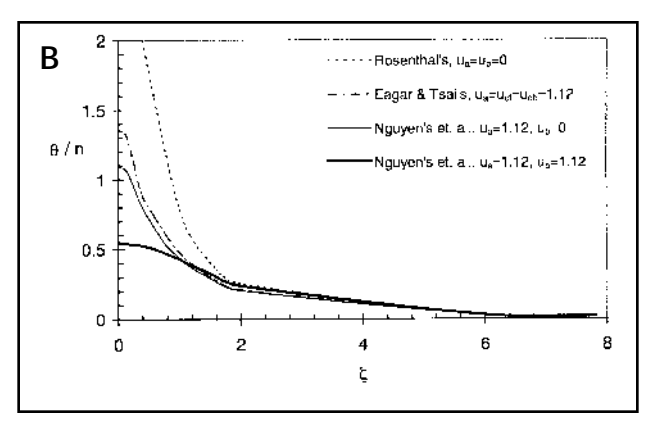


Fig. 3 — Maximum dimensionless temperature distribution through the thickness direction ζ : A — The effect of distribution parameter u_a : B — the effect of distribution parameter u_b .

Furthermore, the solutions for the double ellipsoidal heat source can be converted into dimensionless form by using the following dimensionless variables as recommended by Christensen's method (Ref. 7): $\xi = vx/2a$, $\psi = vy/2a$, $\zeta = vz/2a$, $\tau = v^2(t-t')/2a$; $u_a = va_h/(2\sqrt{6}a)$, $u_b = vb_h/(2\sqrt{6}a)$, $u_{cf} = vc_{hf}/(2\sqrt{6}a)$ and $u_{cb} = vc_{hf}/(2\sqrt{6}a)$. Hence Equations 15a, 15b and 15c become

$$\begin{split} \frac{\theta}{n} &= \\ \frac{1}{2\sqrt{2\pi}} \int\limits_{0}^{\frac{\sqrt{2}t}{2a}} \frac{d\tau}{\sqrt{\tau + u_{a}^{2}}\sqrt{\tau + u_{b}^{2}}} \left(\frac{A_{1}}{\sqrt{\tau + u_{cf}^{2}}} + \frac{B_{1}}{\sqrt{\tau + u_{cb}^{2}}} \right) & (16a) \\ where \ A_{1} &= r_{f} \cdot \exp \left(-\frac{\left(\xi + \tau\right)^{2}}{2\left(\tau + u_{cf}^{2}\right)} - \frac{\psi^{2}}{2\left(\tau + u_{a}^{2}\right)} \right) & (16b) \\ B_{1} &= r_{b} \cdot \exp \left(-\frac{\left(\xi + \tau\right)^{2}}{2\left(\tau + u_{cb}^{2}\right)} - \frac{\psi^{2}}{2\left(\tau + u_{a}^{2}\right)} - \frac{\zeta^{2}}{2\left(\tau + u_{b}^{2}\right)} \right) & (16c) \end{split}$$

and n is the operating parameter (Ref. 2) and n = $\rm Qv / (4\pi a^2 pc(T_c-T_o))$ and $\rm T_c$ - is a reference temperature (in this study, $\rm T_c$ is selected as melting temperature). Since it was quite reasonable to assume that c_{hf} = a_h and c_{hb} =2 c_{hf} , then Equations 16a, 16b and 16c can be reduced to a much simpler form as

$$\frac{\theta}{n} = \frac{1}{2\sqrt{2\pi}} \int_{0}^{\frac{\sqrt{2}t}{2a}} \frac{d\tau}{\sqrt{\tau + u_{b}^{2}}} \left(\frac{A_{1}}{\sqrt{\tau + u_{a}^{2}}} + \frac{B_{1}}{\sqrt{(\tau + u_{a}^{2})(\tau + 4u_{a}^{2})}} \right) (17a)$$
where $A_{1} = r_{f} \cdot \exp\left(-\frac{(\xi + \tau)^{2} + \psi^{2}}{2(\tau + u_{a}^{2})} - \frac{\zeta^{2}}{2(\tau + u_{b}^{2})} \right) (17b)$

$$B_{1} = r_{b} \cdot \exp\left(-\frac{(\xi + \tau)^{2}}{2(\tau + 4u_{a}^{2})} - \frac{\psi^{2}}{2(\tau + u_{a}^{2})} - \frac{\zeta^{2}}{2(\tau + u_{b}^{2})} \right) (17c)$$

It can be seen from Equations 17a, 17b and 17c that the transient temperature at any point (ξ , ψ , ζ) depends on the three parameters: operating parameter (n) describing the magnitude and the in-

tensity of the heat input and two dimensionless heat source shape parameters (u_a and u_b) representing the width and depth of the ellipsoidal heat source. A numerical procedure is used in this study to investigate the effect of these three parameters on the maximum temperature at various positions, and the results are reported below.

It is also worth noting here that for a special case when $b_h = 0$ and $c_{hb} = c_{hf} = a_h$, Equations 16a, 16b and 16c would give the same form as the dimensionless transient temperature solution subjected to 2-D Gaussian distribution surface heat source published by Eagar and Tsai (Ref. 2).

Numerical Results

Effect of Heat Source Parameters u_a and u_b on the Peak Temperature Distribution

In this study, a numerical procedure is applied to find solutions for the transient temperature field as described by Equation 17a, b and c for the double ellipsoidal distributed heat source. A com-

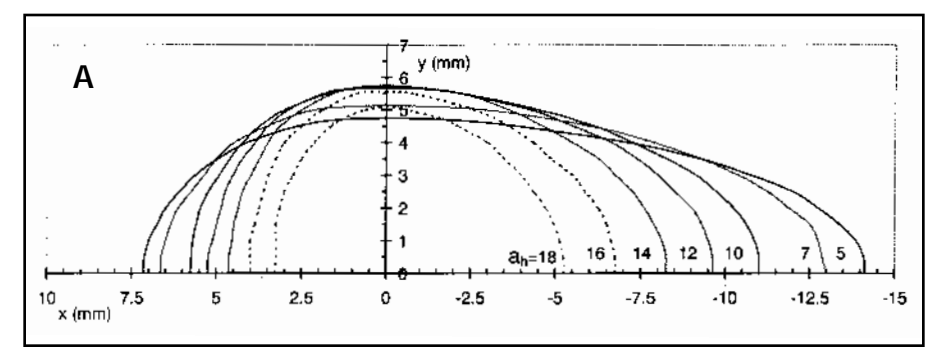
puter program is written in FORTRAN 77 to facilitate the integral calculation and to allow for rapid calculation of transient temperature as well as maximum temperature of any point of interest. Since the solution was obtained for a semi-infinite body, the mirror method, which combines the temperature distribution in case of infinite thickness and its reflected image, was adopted for plate thickness consideration. By using this method, it was assumed that there is no convective heat flow through the upper and lower surface of the plate (Ref. 1).

In order to illustrate the solutions for peak temperature distribution along the transversal and through-thickness direction corresponding to various parameters of the double ellipsoidal distributed heat source, ranges of the source distribution parameters should be selected. Noting there is a similarity between the dimensionless distribution parameters of Eagar and Tsai's solution ($u = v\sigma/2a$) and of this 3-D solution u_a and u_b ($u_a = va_b/(2\sqrt{6} a)$; $u_b = vb_h/(2\sqrt{6} \ a)$). By putting $\sigma_a = a_h/\sqrt{6}$ and $\sigma_b = b_b/\sqrt{6}$, it would bring u_a and u_b into the same form as of u, where σ_a and σ_b are heat source distribution parameters in ψ and ζ directions, respectively.

Since both σ_a and σ represents the width of the heat source, it is quite reasonable to assume that their range of variation would be the same. Fortunately, the range of σ was reported to be between 1.6 and 4 mm for gas tungsten arc welding (GTAW) (Ref. 2). Therefore, if a similar welding heat source is considered, e.g. gas metal arc welding (GMAW), then the range of σ_a could assume to be the same as that of σ . As a result, for a constant welding speed of 5 mm/s and for a diffusivity of base metal a = 6.393 mm²/s, u_a would be varied between 0.6 and 1.6 (0.6 $\leq u_a \leq$ 1.6).

However, the range of σ_b could be from zero (in the case of surface welding) to the maximum value of σ_a or even greater, depending on the characteristics of the considered heat source. In general, most of the common heat source would be more effective in the surface direction (ξ and ψ) than the depth direction (ζ), *i.e* $0 \le \sigma_b \le \sigma_a$. Hence, for the solution demonstration purpose in this study, the range of u_b is selected to be between 0 and 1.12 ($0 \le u_b \le 1.12$).

In the case when $u_a = u_b = 0$, the 3-D Gaussian heat source has no width and the solution given by Equations 17a, b and c would reduce to Rosenthal's solution of point heat source (Ref. 1). In addition, when $u_b = 0$ and $u_a = u_{cf} = u_{cb} = u > 0$, the 3-D Gaussian heat source becomes Eagar and Tsai's solution for a 2-D Gaussian normally distributed heat source (Ref. 2). Therefore, in this study,



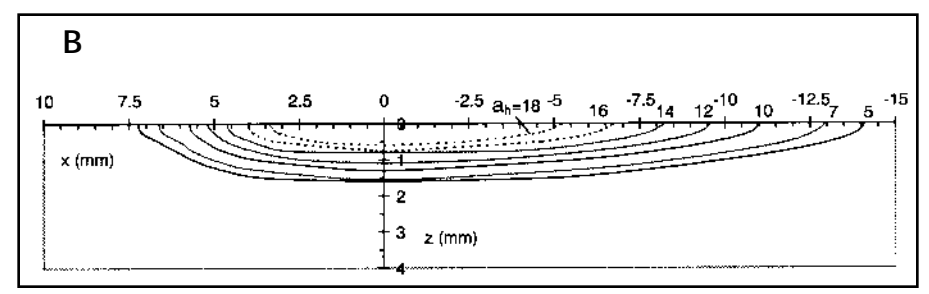


Fig. 4 — Effect of a_h on the predicted weld pool geometry (b_h = 2 mm, c_{hf} = 7 mm, η = 0.8, c_{hb} = $2c_{hf}$): A — Top view of the weld pool; B — longitudinal cross section.

the numerical results are presented for various combinations of distribution parameters u_a and u_b within their ranges and for two particular cases ($u_a = u_b = 0$ and $u_b = 0$; $u_a = u_{cf} = u_{cb} = u > 0$) for comparison.

Figures 2 and 3 show the distributions of the dimensionless maximum temperature along the transversal direction ψ and through-the-thickness direction ζ , respectively, subjected to the variations of u_a and u_b . Both Rosenthal's and Eagar and Tsai's solutions for similar distribution parameters are also plotted for comparison. These figures also provide information about the shapes of the weld pool (width and depth) and of the heataffected zone (HAZ) when the value of (θ/n) corresponds to the melting temperature ($\theta = 1$) and transformation temperature ($\theta = 0.47$), respectively. However, the effect of the heat source parameters on the predicted shape of the weld pool is reported in more detail in the next paragraph.

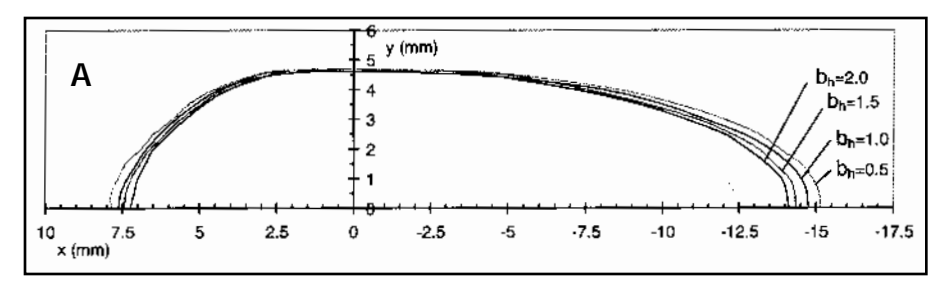
Figure 2A shows the maximum temperature near the weld centerline (ψ <1.4) decreases as the u_a increases while u_b was kept unchanged (u_b =0.32). However, at a further distance from the weld centerline (ψ >1.4), maximum temperature increases as the u_a increases. This behavior of the distribution of maximum temperature is reflected in the predicted weld widths due to variation of u_a . This means that for low value of operating parameter n (n <1.8, which would produce θ/n higher than 0.55 at the weld pool boundary) the predicted weld width de-

creases as u_a increases as in Fig. 2A. However, for high operating parameters (n > 1.8), the predicted weld width increases as u_a increases.

A physical explanation for these behaviors of maximum temperatures is that the larger the width of the heat source, the smaller its heat flux density, and if the heat flux is small enough, it could result in a situation with no melting zone when the peak temperature reduces to less than the melting temperature of the base material. However, when the heat source is strong enough, the peak temperature increases as u_a increases, and the larger weld width is expected.

Figure 2 also shows that for the same value of distribution parameter ($u_a = 1.2$), the present 3-D solution gives a lower predicted maximum temperature than that of Eagar and Tsai's solution, *i.e.*, results in lower predicted weld width. On the other hand, at the vicinity of the weld centerline (ψ <1.4), the present solution gives a much lower predicted maximum temperature than that of the Rosenthal's solution. However, at a further distance from the weld center line (ψ >1.4), the present solution gives only a slightly higher maximum temperature than that of Rosenthal's solution.

In contrast, Fig. 2B shows a unique trend of the maximum temperature behavior due to u_b variation, while u_a was kept unchanged (u_a = 1.12). It shows that for all values of n, the maximum temperature decreases as the u_b increases. This behavior may be due to the fact that re-



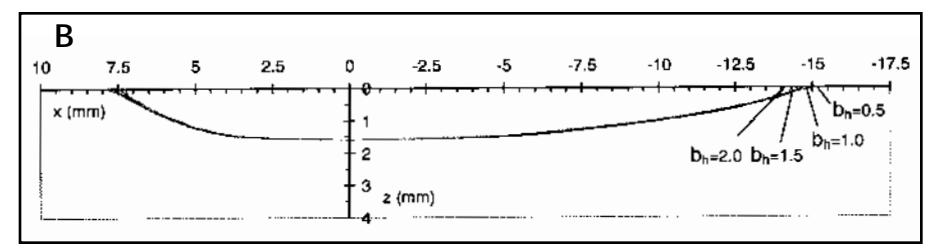
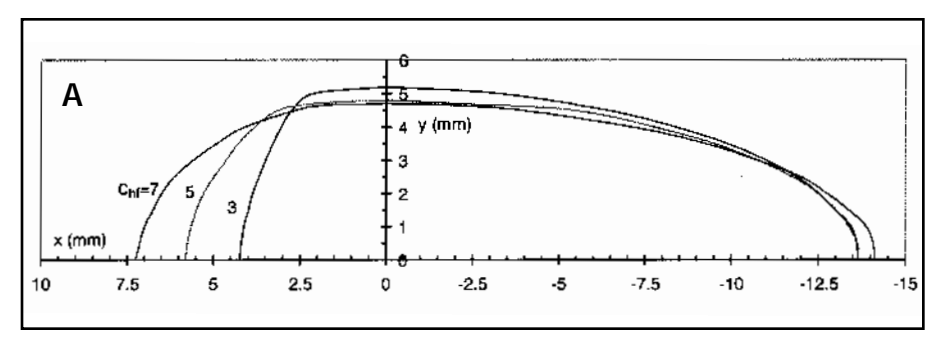


Fig. 5 — Effect of b_h on the predicted weld pool geometry (a_h = 5 mm, c_{hf} = 7 mm, η = 0.8, c_{hb} = $2c_{hf}$): A — Top view of the weld pool; B — longitudinal cross section.



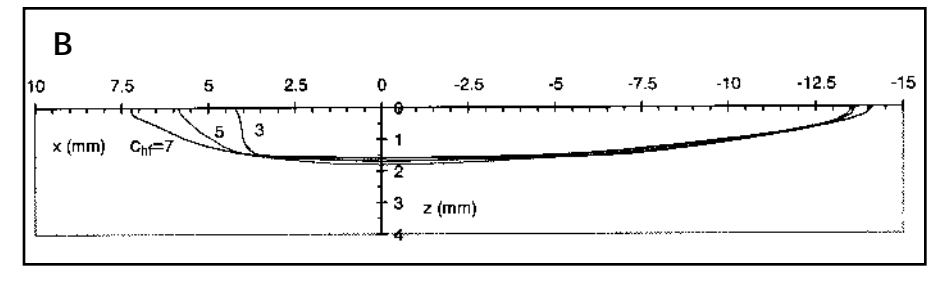


Fig. 6 — Effect of c_{hf} on the predicted weld pool geometry (a_h = 5 mm, b_h = 2 mm, η = 0.8, c_{hb} = $2c_{hf}$): A — Top view of the weld pool; B — longitudinal cross section.

gardless of the magnitude of the operating parameter, the weld depth increases as u_b increases, hence, the weld width decreases due to the constant volume of the melting material induced by constant heat input.

Figure 2A and B also shows that the present 3-D Gaussian heat source solution does not predict the infinite peak temperature at the weld centerline while the Rosenthal solution does. This trend could also be found in Eagar and Tsai's 2-D heat source solution; however, it would predict much higher peak temperature at the weld centerline than that of the 3-D Gaussian heat source solu-

tion, with a similar distribution parameter as shown in Figs. 2A and B.

Figure 3A and B shows that the maximum temperature distribution through the thickness direction ζ as a function of distribution parameter u_a (or u_b) while u_b (or u_a) was kept unchanged, respectively. Two other peak temperature curves of Rosenthal's and Eagar and Tsai's solutions are also plotted for comparison. It can be seen from Fig. 3A that as the u_a increases the peak temperature decreases throughout the thickness direction; hence, the predicted weld pool depth decreases as u_a increases. The predicted weld pool depth by the present solution

is smaller than that by both Eagar and Tsai's and Rosenthal's solutions.

Figure 3B shows a slightly different behavior of maximum temperature distribution throughout the thickness direction ζ due to u_b variations. It can be seen from Fig. 3B that as the u_b increases, the peak temperature decreases at a relatively shallow dimensionless depth (ζ <1.1). However, at a deeper depth (ζ >1.1), this trend gradually changed to the reverse direction. The change is not as pronounced as is found for the peak temperature along ψ when u_a is varied as in Fig. 2A.

Figure 3B also shows that the weld pool depth predicted by the present solution is slightly smaller than that predicted by both Eagar and Tsai's 2-D and Rosenthal's solutions. However, for higher values of the operating parameter, the predicted weld pool depths by all the three above-mentioned solutions are comparable.

Effect of Heat Source Parameters on the Predicted Weld Pool Geometry

In this section, a similar calculating procedure was employed but Equations 15a, b and c were used instead. This would give us a better image of how various heat source parameters (a_h , b_h , c_{hf} , c_{hf} and η) will affect the predicted shape of the weld pool. The following material properties were used: c = 600 J/kg/°C; k = 29 J/m/s/°C and $\rho = 7820 \text{ kg/m}^3$. The arc parameters used were U = 26 V, I = 230 A and v = 30 cm/min.

Figures 4A and B show the effect of the heat source parameter a_h on the top view of the weld pool shape and its longitudinal cross section, respectively, while other heat source parameters are kept unchanged ($b_h = 2 \text{ mm}, c_{hf} = 7 \text{ mm},$ $\eta = 0.8$) and the ratio of c_{hb} and c_{hf} was unchanged, too $(c_{hb}/c_{hf} = 2)$. Figure 4A shows that as a_h increases from 5 to 14, the shape of the weld pool tends to be shorter and fatter, i.e., its length decreases but its width increases. However, as a_h increases beyond a certain value (a_h > 14 mm), the weld pool becomes shorter and thinner. This behavior of the heat source can also be explained by the nature of the distributed heat source. This means that the higher the value of a_h , the weaker the density of heat flux. At the lower values of a_h ($a_h < 14$ mm), when the corresponding density of heat flux is still high enough, the width of the weld pool increases as a_h increases and the weld pool length decreases for the same amount of heat input. At a higher value of a_h ($a_h > 14$ mm), the density of heat flux decreases substantially, and the same heat input will result in a lesser amount of melted metal, i.e., the smaller

Table 1 — Chemical Composition of the Materials												
Materials	С	Si	Mn	Р	S	Cu	Ni	Cr	Мо	V	В	Ti + Zr
HT-780 MIX-60B												

the Materials								
Materials	Yield	Ultimate	Elongation					
	Strength	Tensile	(%)					
	C (1.1D.)	Strength						
	S_y (MPa)	S_u (MPa)						
HT-780	821	859	31					
MIX-60B	601	662	28					

Table 2 — Mechanical Properties of

the Materials

size of the weld pool. However, Fig. 4B shows the size of the weld pool in longitudinal cross section decreases as a_h increases, *i.e.*, the pool depth decreases as a_h increases.

Figure 5A and B shows the effect of the heat source parameter b_h on the top view of the weld pool shape and its longitudinal cross section while the other heat source parameters are unchanged $(a_h = 5 \text{ mm}, c_{hf} = 7 \text{ mm}, \eta = 0.8)$ and $c_{hb}/c_{hf} = 2$. It can be seen from that figure there is an insignificant influence of b_h on the pool depth while the other parameters were unchanged. Its influence on the top view of the weld pool shape is minor. The weld pool length slightly decreases as b_h increases from 0.5 to 2 mm, but the width of weld pool is unchanged.

Figure 6A and B shows the effect of the heat source parameter c_{hf} on the top view of the weld pool shape and its longitudinal cross section while other heat source parameters are unchanged ($a_h = 5$ mm, $b_h = 2$ mm, $\eta = 0.8$) and $c_{hb}/c_{hf} = 2$. It can be seen from this figure that as c_{hf} increases the weld pool width decreases, but its length increases. The increase of weld pool length is more pronounced at its front half than at its back half. The decrease of the weld pool width is at a much lower magnitude. The behavior of top view of the weld pool shape subjected to the c_{hf} is reflected on its longitudinal cross section, as shown in Fig. 6B; however, the effect of c_{hf} on the weld pool depth is insignificant.

Figure 7 shows the effect of the efficiency of heat source η on the weld pool shape. It's clear from this figure that the higher the heat source efficiency the bigger the weld pool, as is expected. However, the effect of η on the weld pool is more pronounced at its back half than that at its front half or at its side.

Experimental Verification

Specimen and Materials

The specimens used for transient temperature measurement were square HT-780 plates 240 x 240 x 20 mm with the chemical composition and mechanical properties shown in Tables 1 and 2, respectively. Two perpendicular linear segments of weld beads run on top of the steel plate are shown in Fig. 8. A welding robot was used to run GMA weld

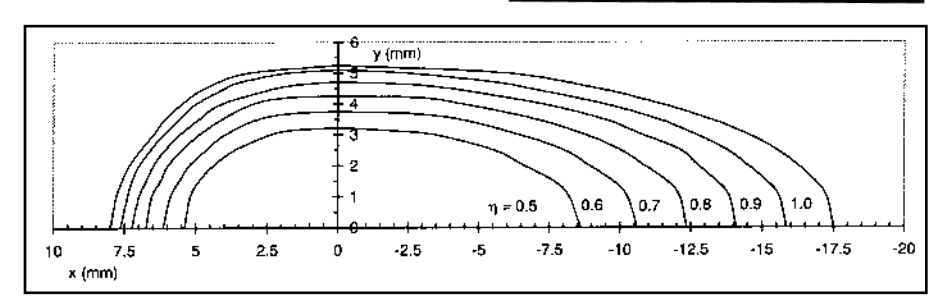


Fig. 7 — Effect of η on the predicted weld pool geometry (a_h = 5 mm, b_h = 2 mm, c_{hf} = 7 mm, c_b = $2c_f$)

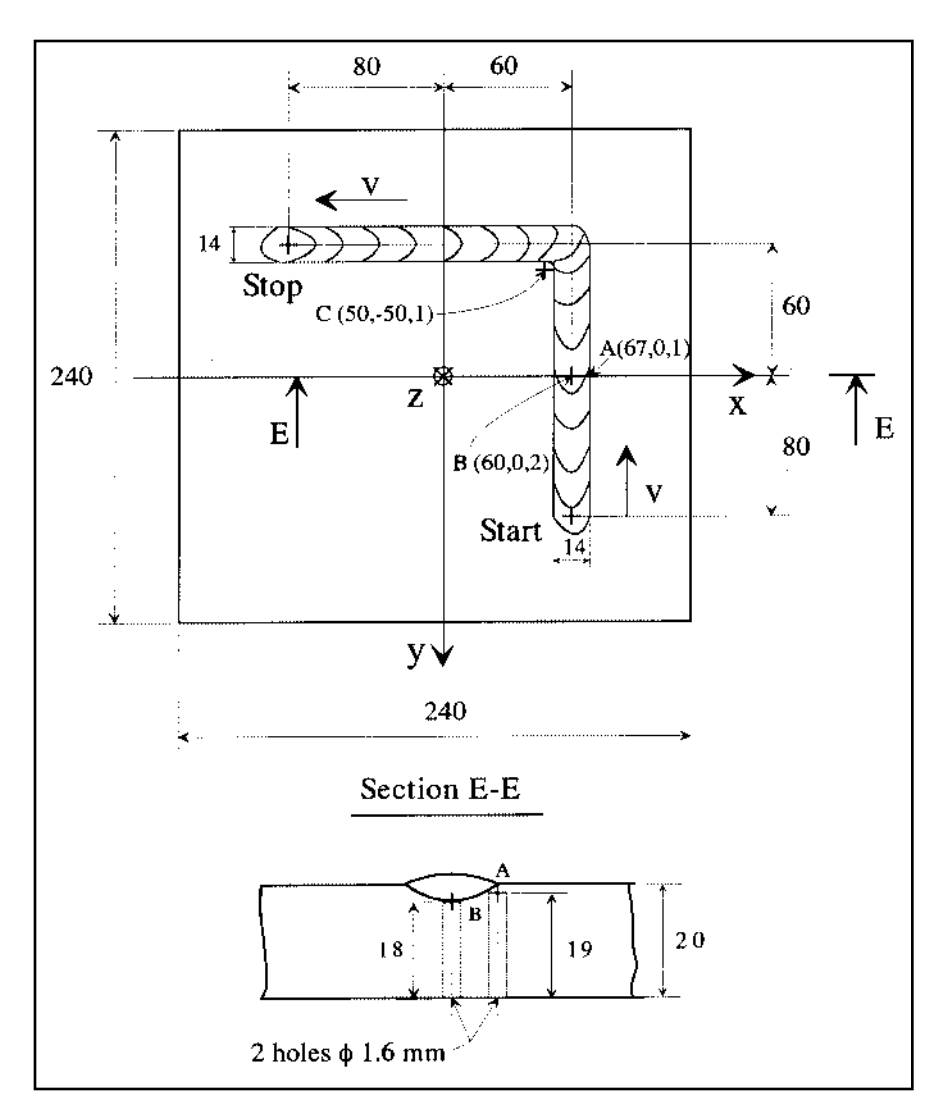


Fig. 8 — Specimen for transient temperature measurement.

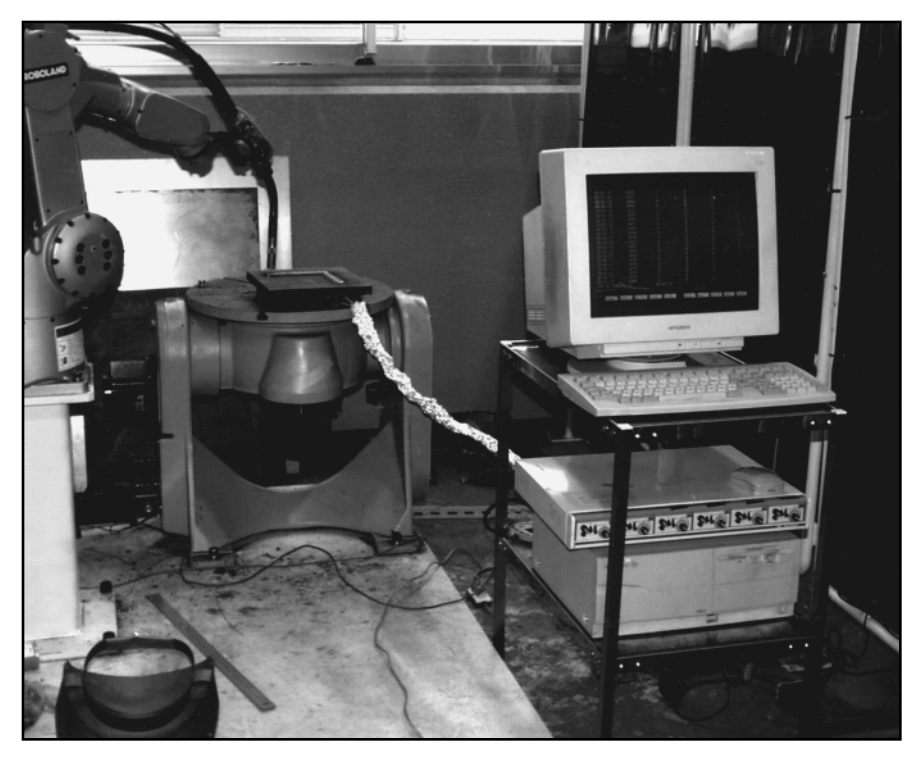
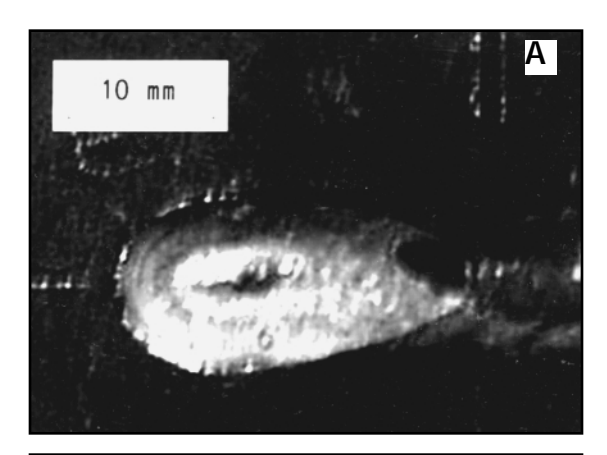


Fig. 9 — Experimental setup for temperature measurement.



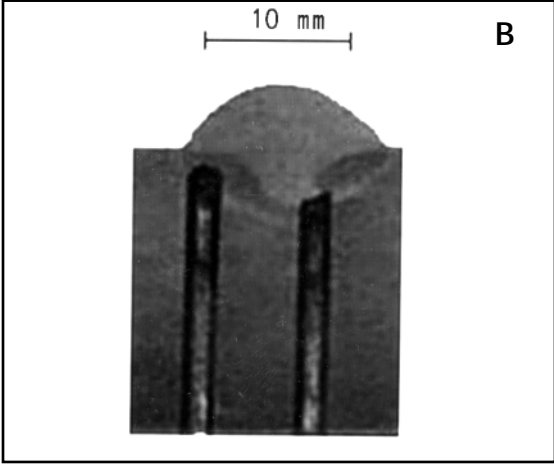


Fig. 10 — Geometry of the weld pool: A — Top view; B — tranversal cross section.

beads on the plates with the following welding parameters: U = 26 V, I = 230 A and v = 30 cm/min. A shielding gas mixture of 80% argon 20% CO₂ was supplied at 20 L/min. The filler metal was MIX-60B; its chemical composition and mechanical properties are given in Tables 1 and 2, respectively. Three platinium and platiniumrhodium CC thermocouples (Ref. 9) were used to measure the transient temperature at various interest points A, B and C as shown in Fig. 8. These points were selected to monitor the transient temperatures around the weld toe, the bottom of the weld pool (weld root) and the corner of the weld interface segments to get necessary data for the verification of the analytical solutions.

Three holes with a diameter of 1.6 mm were drilled from the back surface of the test plate with their depths corresponding to the positions for points of interest A, B and C. Thermocouples were spot welded to the bottom of these holes to avoid the

possible damage caused by the welding heat source of a percussion welding machine. Thermocouples were then connected to an isolation-type voltage amplifier, the output of which was connected to a PC with a built-in analogue-digital converter card. A picture of the experimental setup for temperature measurement is shown in Fig. 9.

A computer program was written and used to control input and output signals. It provided the necessary data for the measured transient temperature by using the available calibration data for CC thermocouples.

Model Calibration with the Measured Weld Pool Geometry

The geometry of the weld pool generated from the tests were reported by means of photos taken for the weld pool shape at the surface of the welded plate and at its transversal cross section (E-E in Fig. 8) as shown in Fig. 10. The two drilled holes for thermocouples at corresponding points A and B (Fig. 8) were also captured by these photos. The positions of the thermocouples at these holes were relocated and used for the calculation. The data for the weld pool profiles were measured directly from the photographs using the scales of the Adobe Photoshop program.

Figure 11A and B shows comparisons between the measured and predicted data for the top view of the weld pool shape on welded plate and its transversal cross section. The predicted data were calculated using the following parameters of the heat source, which provide the best fit with the measured data: $a_h = 10$ mm, $b_h = 2$ mm, $c_{hf} = 10$ mm, $\eta = 0.85$ and $c_{hb} = 2c_{hf}$. These parameters were successfully selected based on their effect on the weld pool geometry reported previously. The heat transfer material properties used for the calculation were selected for HT-780 steel based on its ranges (Ref. 8), and they were the same as previously reported.

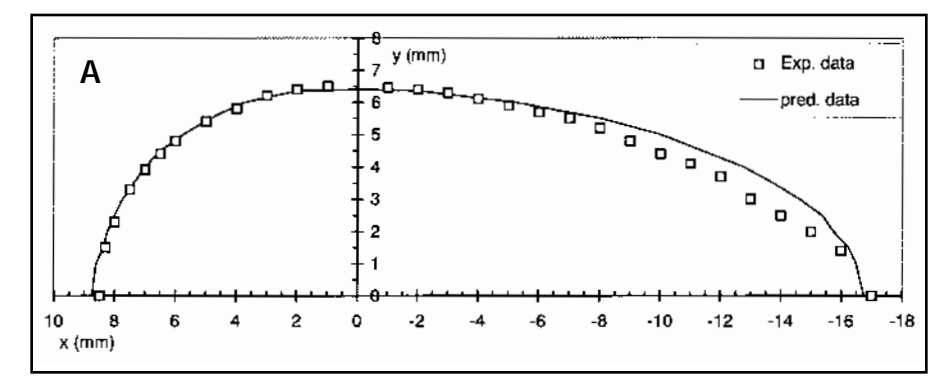
It is obvious from that figure that the present 3-D heat source model can give very good agreements with the measured data given so that suitable parameters of the heat source can be carefully selected. This means that the predicted model can be easily calibrated with the experimental data by selecting its heat source parameters. Then, it can be used for various simulation purposes. However, Fig. 10B also shows the present model fails to predict the complex shape of the weld pool in the transversal cross section. This is expected since many simplified assumptions have been used for the development of the present analytical solution.

Transient Temperature Results

Figure 12 shows the measured transient temperatures at three points representing the weld toe (A), weld root (B) and corner point (C) as illustrated in Fig. 8 and the corresponding predicted transient temperatures by the present 3-D power density heat source solution. Transient temperatures are calculated using the solution obtained for double ellipsoidal distributed heat source.

The parameters of the double ellipsoids used for the calculation in this section were taken from the result obtained previously regarding the best fit of weld pool geometry ($a_h = 10 \text{ mm}$, $b_h = 2 \text{ mm}$, $c_{hf} = 10 \text{ mm}$, $c_{hb} = 20 \text{ mm}$ and $\eta = 0.85$), and the same heat transfer material properties were used (c = 600 J/kg/°C; k = 29 J/m/s/°C; $\rho = 7820 \text{ kg/m}^3$ and, therefore, $a = k/c\rho = 6.181 \times 10^{-6} \text{ m}^2/\text{s}$).

It can be seen from Fig. 12 that the measured temperatures of points A and B increased almost immediately after the welding arc passed their position. The maximum temperature of point B is higher than that of A, as expected, because B is located closer to the weld pool boundary than A. Figure 12 also shows the maximum measured transient temperature of point C is lower than that of point A and B, as expected, due to the fact that position C was much farther from the weld pool than that of A or B (about 3 mm from the weld toe). It is also worth noting here a delayed increase in temperature of point C compared with A and B, due to its particular position and the welding path, was successfully recorded. An expected transition zone in the transient temperature of point C, due



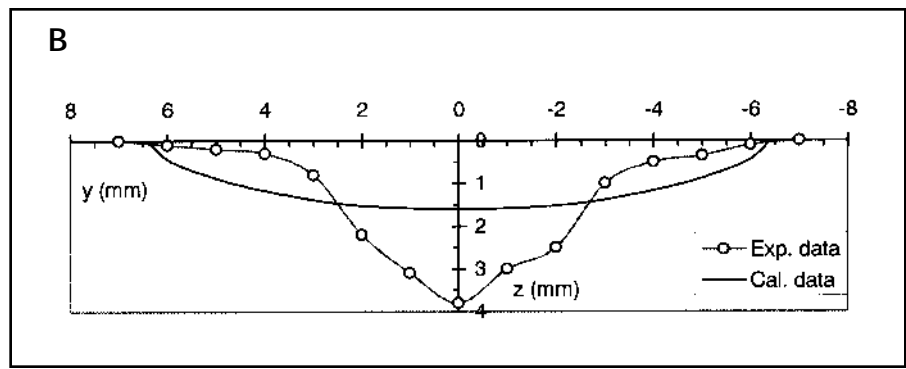


Fig. 11 — Comparisons between calculated and measured data of the weld pool: A — Top view of the weld pool; B — longitudinal cross section.

to its corner position, was successfully recorded, as shown in Fig. 12. Furthermore, Fig. 12 also shows there is a very good agreement between the predicted and measured transient temperatures for all three points A, B and C. The shape and the magnitude of the predicted temperatures were expected and were very close to the measured ones. The transition zone in the temperature history of corner point C due to the welding path was successfully simulated by the numerical calculation.

Figure 13 shows another set of measured temperature data compared with the one shown in Fig. 12. It can be seen from Fig. 13 the repeatability of the measured transient temperature is very good in terms of both shape and magnitude. The difference in the peak temperature at the weld toe, weld root and the corner positions is less than 100°C, which is quite acceptable for high-temperature gradients at these positions. This temperature difference also incorporated the unavoidable experimental errors in

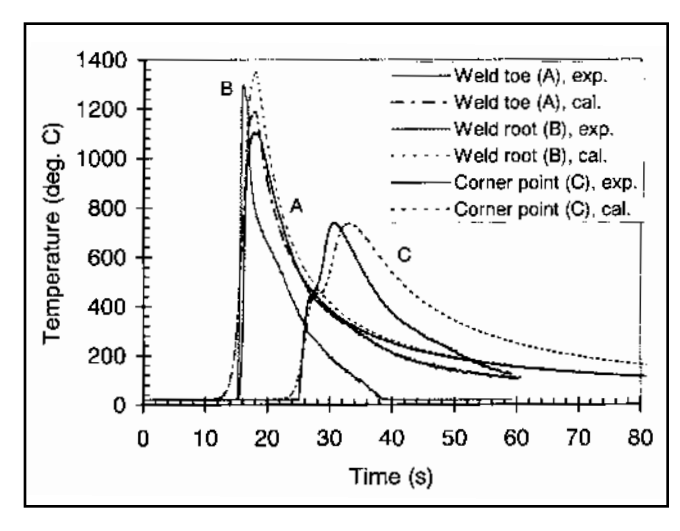


Fig. 12 — Comparison between calculated and measured transient temperatures.

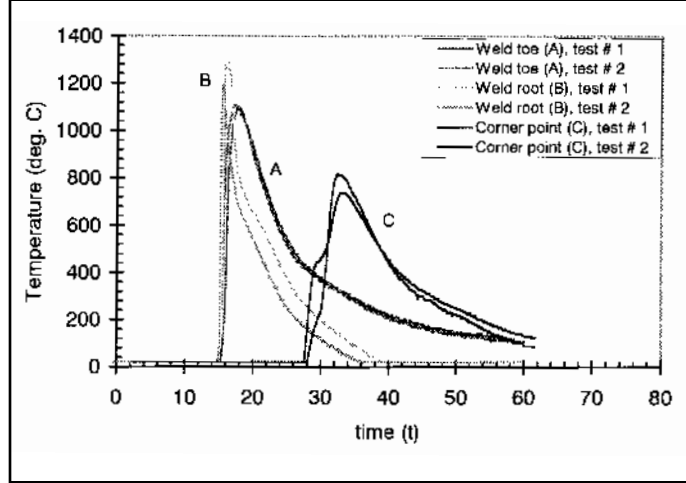


Fig. 13 — Repeatability of the measured transient temperatures.

locating the hole depths to which the thermocouples were bonded.

It can be further noted from Fig. 13 the transition zone of the corner point temperature of test No. 2 is not very distinctive from that of test No. 1. This may be due to a slight change in its relative position to the corner of the weld path. However, both measured temperatures of point C (test Nos. 1 and 2) agree reasonably well with each other.

From the results shown in both Figs. 12 and 13, it can be concluded this new analytical solution could offer a very good prediction for the transient temperatures near the weld pool, and it is able to simulate the complicated weld path as well.

Conclusions

In this study, analytical solutions for the transient temperature field of a semi-infinite body subjected to 3-D power density moving heat sources (such as semi-ellipsoidal and double ellipsoidal heat sources) were found and experimentally validated. Also, it was shown the analytical solution obtained for double ellipsoidal heat source was a general one that can be reduced to semi-ellipsoidal, semi-sphere, 2-D Gaussian-distributed heat source and the classical instant point heat source.

The analytical solution for the double ellipsoidal heat source was used to calculate transient temperatures at three selected points in a steel plate that is subjected to two perpendicular linear welded segments on its surface. Both the numerical and experimental results from this study have showed that the present analytical solution could offer a very good prediction for the transient temperatures near the weld pool, as well as simulate the complicated welding path. Furthermore, very good agreement between the calculated and measured temperature data indeed shows the credibility of the newly found solution and its potential application for various simulation purposes, such as thermal stress analysis, residual stress calculations and microstructure modeling.

Acknowledgments

This work has been sponsored by the Science and Technology Agency (STA) Research Fellowship program, which is administered by JISTEC. The authors would like to express their thanks to Dr. Okada for his advice in the temperature measurement and Drs. Hiraoka and Nakamura for their valuable support by making their Daihen welding robot and measuring system available for this project.

References

- 1. Rosenthal, D. 1941. Mathematical theory of heat distribution during welding and cutting. *Welding Journal* 20(5): 220-s to 234-s.
- 2. Eager, T. W., and Tsai, N. S. 1983. Temperature fields produced by traveling distributed heat sources. *Welding Journal* 62(12): 346-s to 355-s.
- 3. Jeong, S. K., and Cho, H. S. 1997. An analytical solution to predict the transient temperature distribution in fillet arc welds. *Welding Journal* 76(6): 223-s to 232-s.
- 4. Goldak, J., Chakravarti, A., and Bibby, M. 1985. A Double Ellipsoid Finite Element Model for Welding Heat Sources, IIW Doc. No. 212-603-85.
- 5. Painter, M. J., Davies, M. H., Battersby, S., Jarvis, L., and Wahab, M. A. 1996. A literature review on numerical modelling the gas metal arc welding process. *Australian Welding Research*, CRC. No. 15, Welding Technology Institute of Australia.
- 6. Carslaw, H. S., and Jaeger, J. C. 1967. *Conduction of Heat in Solids*, Oxford University Press, Cambridge, U.K., pp. 255.
- 7. Christensen, N., Davies, V., and Gjermundsen, K. 1965. The distribution of temperature in arc welding. *British Welding Journal* 12(2): 54–75.
- 8. Radaj, D. 1992. Heat effects of welding: temperature field, residual stress, distortion. *Springer-Verlag*, pp. 28
- 9. Japanese Industrial Standard 1995. *Thermocouples*, JIS C 1602-1995, Japanese Standard Association, Japan.

American Welding Society — Detroit Section International Sheet Metal Welding Conference IX October 18–20, 2000 Detroit, Michigan

The international Sheet Metal Welding Conference is the premiere technical conference dedicated to joining methods for thinsheet fabrication. You are invited to consider writing and presenting a technical paper for this conference. In order to allow for review and possible selection by the Technical Committee, a 500–1000 word abstract, along with a completed Author Application Form must be submitted to one of the Technical Committee Chairmen by November 14, 1999. To facilitate access to your abstract, please submit it in a format that is compatible with MS Word 6/97.

Typical categories for the papers may include:

- Resistance Welding Processes
- Arc Welding Advances
- Laser Welding
- Innovative Processes
- Process Monitoring and Control

- Coated Materials
- Welding Light-Weight Materials
- Welding High-Strength Steel
- Welding Tubular Structures
- Application Studies

The paper must be related to sheet metal alloys and/or joining processes used in manufacturing of commerical products. It is not a requirement that your presentation be an original effort. Case histories, reviews and papers that have been previously published or presented will be considered as long as they are pertiment to the general interests of the conference attendees.

Authors must submit a manuscript to the Committee by July 17, 2000. Please submit an author application form along with a 500–1000 word abstract by November 14. The form can be downloaded through www.awsdetroit.org or www.ewi.org. Send it and the abstract to the following: Menachem Kimchi, AWS Technical Chairman, EWI, 1250 Arthur E. Adams Drive, Columbus, OH 43221, Phone: (614) 688-5001, or e-mail menachem_kimchi@ewi.org.